Correlation studies of the ^{5}H spectrum

M. S. Golovkov,[1] L. V. Grigorenko,[1] A. S. Fomichev,[1] S. A. Krupko,[1] Yu. Ts. Oganessian,[1] A. M. Rodin,[1] S. I. Sidorchuk,[1] R. S. Slepnev,[1] S. V. Stepantsov,[1] G. M. Ter-Akopian,[1] R. Wolski,[1,2] M. G. Itkis,[1] A. S. Denikin,[1] A. A. Bogatchev,[1] N. A. Kondratiev,[1] E. M. Kozulin,[1] A. A. Korsheninnikov,[3,*] E. Yu. Nikolskii,[3,*] P. Roussel-Chomaz,[4] W. Mittig,[4] R. Palit,[5] V. Bouchat,[6] V. Kinnard,[6] T. Materna,[6] F. Hanappe,[6] O. Dorvaux,[7] L. Stuttgé,[7] C. Angulo,[8] V. Lapoux,[9] R. Raabe,[9] L. Nalpas,[9] A. A. Yukhimchuk,[10] V. V. Perevozchikov,[10] Yu. I. Vinogradov,[10] S. K. Grishechkin,[10] and S. V. Zlatoustovskiy[10]

[1]*Flerov Laboratory of Nuclear Reactions, JINR, Dubna RU-141980, Russia*

[2]*The Henryk Niewodniczański Institute of Nuclear Physics, Kraków, Poland*

[3]*RIKEN, Hirosawa 2-1, Wako, Saitama 351-0198, Japan*

[4]*GANIL, BP 5027, F-14076 Caen Cedex 5, France*

[5]*Gesellschaft fur Schwerionenforschung (GSI), D-64291 Darmstadt, Germany*

[6]*Université Libre de Bruxelles, PNTPM, Bruxelles, Belgium*

[7]*Institut de Recherches Subatomiques, IN2P3/Université Louis Pasteur, Strasbourg, France*

[8]*Centre de Recherches du Cyclotron, Université catholique de Louvain, B-1348 Louvain-La-Neuve, Belgium*

[9]*DSM/DAPNIA/SPhN, CEA Saclay, F-91191 Gif-sur-Yvette Cedex, France*

[10]*RNFC – All-Russian Research Institute of Experimental Physics, Sarov, Nizhni Novgorod Region, Ru-607190, Russia*

(Received 29 August 2005; published 20 December 2005)

The nuclear system ^{5}H was studied using the ^{3}H$(t, p)^5$H transfer reaction at a laboratory energy of 57.7 MeV and small center of mass angles. The energy and angular correlations among the ^{5}H decay fragments were obtained by complete kinematical reconstruction. A broad structure in the ^{5}H missing mass spectrum above 2.5 MeV with a typical width of several MeV was identified as a mixture of $3/2^+$ and $5/2^+$ states. Analysis of interference patterns observed in the measured angular correlations disclosed the $1/2^+$ ground state of ^{5}H concealed in the smooth missing mass spectrum. The deduced values for the resonance energy and width are $E_{\text{g.s.}} \approx 1.8$ MeV and $\Gamma_{\text{g.s.}} \approx 1.3$ MeV. The estimated cross sections for population of the ground state and the doublet of excited states at $\theta_{\text{c.m.}} = 5^\circ - 10^\circ$ are 150 ± 50 μb/sr and 4.6 ± 2 mb/sr, respectively.

DOI: 10.1103/PhysRevC.72.064612 PACS number(s): 25.10.+s, 25.55.Hp, 27.10.+h, 24.50.+g

I. INTRODUCTION

Modern advances in experimental techniques revived interest in the studies of superheavy hydrogen isotopes, ^{5}H [1–6] and ^{7}H [7,8]. The recent experimental results on ^{5}H are controversial, providing the ground state (g.s.) position to be 1.7–1.8 MeV above the $t + n + n$ threshold [2,3], or about 3 MeV [4], or even higher [1,5]. Recent theoretical estimates [9–13] are sensitive to model assumptions and also give diverse predictions for this system.

Experiments mentioned above utilized different types of reactions having definite advantages and disadvantages. The proton pickup reaction ^{6}He$(p,^2$He$)^5$H used in Ref. [2] is expected to populate predominantly the g.s. of ^{5}H due to the similarity between the structures of ^{6}He and ^{5}H. There is also evidence in the data that the angular momentum transfer $\Delta L = 0$ dominates in this reaction. Meister *et al.* [4] have studied the ^{5}H continuum via the ^{6}He fragmentation on carbon. The domination of the ^{5}H g.s. population is also expected in this case, again due to structure similarity and to the fact that the $\Delta L = 0$ selection is a typical feature for this class of reactions. In the two-neutron transfer reaction ^{3}H$(t, p)^5$H [3,6] the excited $3/2^+$ and $5/2^+$ states are more likely to be populated because of the "angular momentum mismatch." In contrast, in the pion absorption reaction ^{9}Be$(\pi^-, pt/dd)^5$H [5] no angular momentum selectivity is expected and all the low-lying states should be present in the experimental data.

In these experiments the main aim was the search for a peak in the missing (or invariant) mass spectrum of ^{5}H which could be identified as the ground state of ^{5}H. This task is complicated by the fact that the low-lying states in ^{5}H are broad and overlapping. The most recent works [4,6] supplemented the energy spectrum measurements with the correlation studies of decay products. It was shown in Ref. [4] that the correlations among the triton and two neutrons from the ^{5}H decay can be well described by the decay of a $1/2^+$ state. However, it was demonstrated in Ref. [14] that these correlations could also be described assuming the decay of excited states in ^{5}H. The study of more complicated correlations, arising in the two-neutron transfer reaction ^{3}H$(t, p)^5$H due to a specific reaction mechanism, allowed us to identify uniquely the structure observed in the spectrum of ^{5}H above 2.5 MeV as a mixture of excited $3/2^+$ and $5/2^+$ states [6].

The motivation for the present work was the observation of ^{5}H produced in the ^{3}H$(t, p)^5$H reaction in different kinematical conditions as compared with the previous study reported in Ref. [3]. Namely, we investigated this reaction at small center-of-mass angles, corresponding to protons emerging in backward direction in the lab system. This greatly reduced the background from other reaction channels, such as different quasifree scattering processes and the one-neutron transfer. Furthermore, the chosen kinematical region improved the

*On leave from the Kurchatov Institute, Kurchatov sq. 1, Ru-123182 Moscow, Russia.

detection efficiency for triple $p-t-n$ coincidence events associated with the ^{5}H formation and decay.

The following features should be emphasized in the present work.

(i) The experimental data corrected for efficiency are represented in an analytical form, which makes their further theoretical interpretation straightforward.
(ii) For the first time the spin identification in the *system decaying into the three-body continuum* is performed using the correlation technique.

This technique is analogous to the classical approach [15] of α_1-α_2 correlations for the decay of alpha-cluster states in "zero geometry" [16]. In the complicated case of the decay of a three-body system this technique *does not guarantee* the spin identification in a general case, but could be an interesting and important opportunity to be considered.

Results obtained in the present study have been briefly reported in our earlier paper [6]. Here we present the data in more detail and give a complete account for the data analysis together with an extensive discussion. Some quantitative results of this work differ from those given in Ref. [6] due to improvements made in the data analysis.

II. EXPERIMENT

The experiment was performed at the U-400M cyclotron of the Flerov Laboratory of Nuclear Reactions, JINR (Dubna, Russia). A 57.7 MeV triton beam delivered by the cyclotron was transported by the modified beam line of the ACCULINNA separator [17] to a reaction chamber containing a tritium target and charged particle detectors. This beam line was also used to reduce the angular spread and energy dispersion of the primary triton beam to 7 mrad and 0.3 MeV of full width at half maximum (FWHM), respectively. Finally, the triton beam, with a typical intensity of 3×10^7 s^{-1}, was focused in a 5 mm spot on a gas cell of an environmentally safe cryogenic tritium target [18]. The 4 mm thick target cell was filled with tritium to a pressure of 860 mbar and cooled down to 25° K.

The experimental setup is shown in Fig. 1. Slow protons escaping from the target in the backward direction hit on an annular 300 μm silicon detector with an active area of the outer and inner diameters of 82 mm and 32 mm, respectively, and a 28 mm central hole. The detector was installed 100 mm upstream of the target. It was segmented in 32 rings on one side and 32 sectors on the other side providing a good position resolution. The detection threshold for these protons was 1 MeV. A detector telescope intended for charged particles moving in the forward direction was installed 150 and 220 mm downstream of the target cell in two different series of measurements. It consisted of four annular silicon detectors of the same size as the proton detector. The thicknesses of the four detectors beginning from the telescope face side were 300 μm, and 3 times by 1 mm. The two sides of the first, 300 μm detector, were segmented in 16 rings and 16 sectors. Particle identification in the forward telescope was made by standard ΔE–E method. Neutrons were detected by 48 scintillation modules of the time-of-flight (TOF) neutron spectrometer DEMON [19]. The DEMON modules were installed at a distance of 2.5 m from the target and covered an angular range of $\theta_{\rm lab}=5°$–$40°$.

Beam intensity was monitored by low pressure ionization chambers. Three such chambers were distributed along the beam line upstream of the target and one chamber was installed 1 m downstream. Furthermore, a 4 mm thick silicon detector (not shown in Fig. 1) with a diameter of 8 mm was installed just behind the forward detector telescope. Its position corresponded to 5.8° and 7.9° in the lab system in the first and in the second series of measurements, respectively. In the latter case it was possible to resolve the elastic scattering peaks of tritons coming from the target and from the window material. This gave an additional possibility for absolute normalization of the data from the known cross section values.

Detection threshold for slow protons moving in the backward direction (see Fig. 1) defined the range of the accessible ^{5}H energy. To extend to 5.0 MeV the upper limit of this energy range we did not use the ΔE-E identification of protons. This did not result in any confusion. Indeed, due to the kinematical constraints of the $t+t$ collision, only protons and deuterons can be emitted in the backward direction. Since the maximum energy of deuterons does not exceed 1 MeV, all these deuterons should be stopped in the target or in the target window. Thus only protons from the $t+t$ interaction can hit the detector, and particles, other than protons, can only be produced in reactions on the window material. This background was

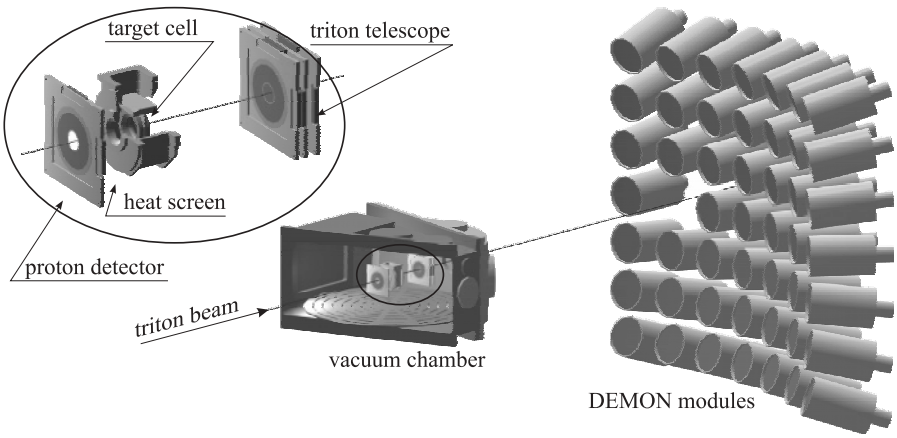

FIG. 1. Experimental setup for the ^{3}H(t, p)^{5}H reaction.

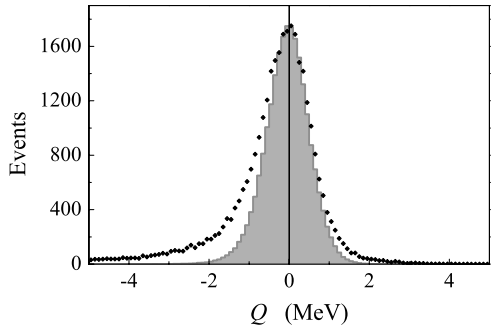

FIG. 2. Distribution of the measured Q value obtained for the ^{3}H$(t, p)^5$H reaction. Experimental data are shown by points, the shadowed histogram shows the MC simulation.

measured in a special run made with an empty target. It was found that the background originating from the reactions on the window material was negligible for the triple $p - t - n$ coincidence event, not more than a few percent of the total number of counts. The analysis of triple $p - t - n$ coincidence events also gave another possibility to identify the reaction channel. For the $t + t \rightarrow p + t + 2n$ reaction channel, these events correspond to complete kinematics conditions, since the parameters of the unobserved neutron can be calculated from the momentum conservation law. By comparison of the total energy in the exit channel with the beam energy one can resolve events coming from the $t + t$ interaction from the background originating from the reactions taking place on the target window material. Figure 2 shows the total energy balance Q for triple coincidence events:

$$Q = \sum_{j=1,2} \left(M_i^{(\mathrm{in})} + E_i^{(\mathrm{in})}\right) - \sum_{j=1\ldots4} \left(M_j^{(\mathrm{out})} + E_j^{(\mathrm{out})}\right) \equiv 0.$$

The experimental data are shown by points, the shadowed histogram presents the Monte Carlo (MC) simulation of the experiment. Some asymmetry of the Q value peak is possibly caused by the scattering of neutrons occurring before their detection. The effect of this phenomenon on the final results of the analysis was found to be not significant. The energy resolution estimated from the MC calculation for the missing mass energy of ^{5}H is 0.4 MeV (FWHM).

The DEMON neutron detector modules allow neutron-gamma separation by the comparison of total and slow components of the light output of the liquid scintillator. The energy calibration of DEMON was made with ^{60}Co and ^{137}Cs γ-sources. Neutron energies were measured by the TOF method. For the time calibration we used the TOF spectrum gated on the coincidence of the particle detection with the γ events in DEMON. Having fixed the complete kinematical conditions in each triple $p - t - n$ coincidence event, we calculated the momentum distribution of the unobserved neutrons emitted in the $t + t \rightarrow p + t + 2n$ reaction channel. Then, the detected four-fold $p - t - n - n$ coincidences gave direct information on the detection efficiency obtained for neutrons. The statistics of four-fold coincidence events was high enough to determine the energy dependence of the neutron efficiency in the whole region of interest.

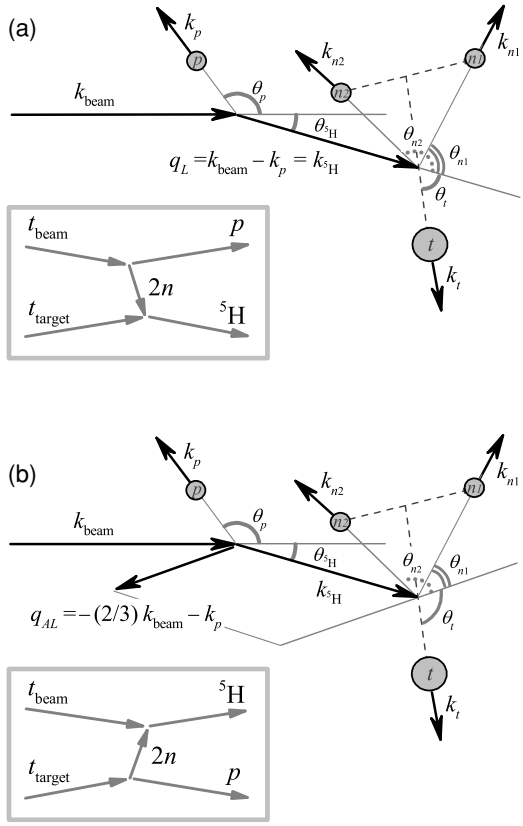

FIG. 3. Kinematical variables for the ^{3}H$(t, p)^5$H reaction. The proton and ^{5}H variables are shown in the laboratory frame, variables for the decay triton and neutrons are presented in the ^{5}H frame. Direction of Z axis in the ^{5}H frame is chosen collinear with the direction of momentum transfer assuming a direct reaction mechanism (see insets). (a) The dineutron is transferred from the beam to the target triton (transferred momentum $\mathbf{q}_L$ is equal to the momentum of ^{5}H in the laboratory frame). (b) The dineutron is transferred from the target to the beam triton. Transferred momentum $\mathbf{q}_{AL}$ is equal to momentum of ^{5}H in the "antilaboratory" frame, where the projectile is in rest. See also discussion in Sec. IV.

III. EXPERIMENTAL DATA

As mentioned above, here we present results obtained for the triple $p - t - n$ coincidence events. Such events uniquely identify the $p + {}^5$H outgoing channel and enables a complete kinematics reconstruction. Data are presented in the center of mass (c.m.) of the $t + 2n$ system, most appropriate for the search for the ^{5}H resonances. We choose the Z axis along the direction of the momentum transfer, $(2/3)\mathbf{k}_{\mathrm{beam}} + \mathbf{k}_p$ [see Fig. 3(b) for notations]. This choice is justified in Sec. IV C. 12 kinematical variables completely describe the four particles (proton, triton, and two neutrons) coming in the exit channel of the reaction. The energy and momentum conservation laws reduce the number of independent variables to eight. Our experimental setup provides a relatively small angular range for the proton registration: $5^\circ < \theta_{\mathrm{c.m.}} < 10^\circ$. One could suppose that all angular distributions are almost uniform within these limits. This expectation was *a posteriori* confirmed by the data analysis. Also nothing should depend on the proton azimuthal angle ϕ_p, due to the azimuthal symmetry

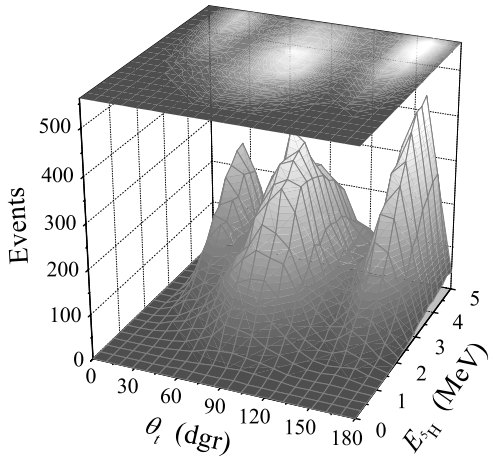

FIG. 4. Distribution of experimental events drawn in the plane $\{E_{^5\mathrm{H}}, \theta_t\}$ for the ^{5}H events detected in the $^3\mathrm{H}(t, p)^5\mathrm{H}$ reaction. The coordinate system is the same as Fig. 3(b).

of the process. Thus, the experimental data are presented as a six-dimensional array of independent variables: The polar and azimuthal angles of the triton (θ_t, ϕ_t) in the ^{5}H c.m. system, the same variables for one of the emitted neutrons (θ_{n1}, ϕ_{n1}), the total energy of ^{5}H $E_{^5\mathrm{H}} = E_{nn} + E_{t-nn}$, and the energy distribution between the subsystems $\varepsilon = E_{nn}/E_{^5\mathrm{H}}$ inside ^{5}H.

As an example of our experimental data, two dimensional plots are shown in Figs. 4 and 5. No correction for the detection efficiency is made. These distributions have very specific features, but the most striking result is the observation of a sharp oscillating pattern in the angular distributions of tritons and neutrons.

In the triton angular distribution (see Fig. 4) three sharp peaks are observed in a broad range of energy $E_{^5\mathrm{H}}$. We will show that the origin of these peaks is the population of excited states in ^{5}H whose structure is dominated by the component with the triton in d-wave. It can be seen that at low $E_{^5\mathrm{H}}$ the "satellite" peaks (backward and forward direction) vanish, and one peak remains at 90°. We will show below that such a change in the distribution is not connected with efficiency, but

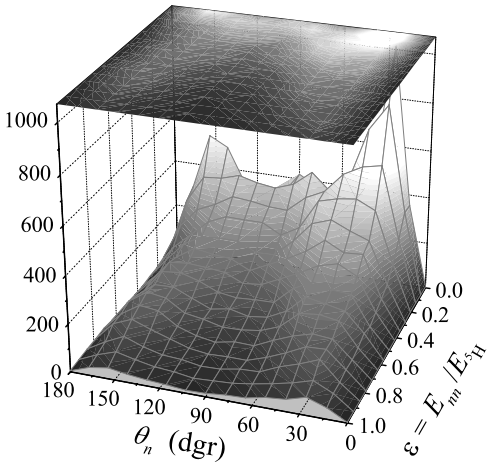

FIG. 5. Experimental ^{5}H events for the $^3\mathrm{H}(t, p)^5\mathrm{H}$ reaction in the plane $\{\varepsilon, \theta_n\}$. The coordinate system is the same as Fig. 3(b).

is the result of the interference of excited states of ^{5}H with the $1/2^+$ ground state.

The main feature of the neutron distribution, shown in Fig. 5, is a strong concentration of probability at low E_{nn} energy. This is clearly connected with a strong $n-n$ final state interaction (FSI). In this part of the spectrum, the angular distribution also has three peaks which are related to the triple-peak distribution of tritons. Indeed, in the limit $E_{nn} \to 0$ the individual motion of neutrons is reduced to the motion of a single dineutron particle, which has the same angular distribution as the triton in the ^{5}H c.m. system. At higher E_{nn} energies, the distribution of neutrons has two peaks. This is a manifestation of the p-wave motion of individual neutrons, which is an expected feature for ^{5}H.

IV. THEORETICAL BACKGROUND

A. Correlations in the transfer reactions

In principle, the strong oscillations observed in the angular distributions of tritons (three peaks) and neutrons (two peaks) could have two explanations. They could either be formed by a specific reaction mechanism only or they could be a manifestation of states in ^{5}H. Calculations performed in the distorted wave Born approximation (DWBA) for the $^3\mathrm{H}(t, p)^5\mathrm{H}$ reaction (see discussion in Sec. VI C and Appendix A) show that the first explanation is highly unlikely and that the population of specific states in ^{5}H is necessary to explain the data. A qualitative discussion of correlations in the transfer reaction in general and of the origin of correlations in our particular case was given in Ref. [6]. The main point is that such a sharp oscillating angular distribution as the one shown in Fig. 4 can be obtained only for very specific conditions. Here we would like to outline briefly the discussion presented in Ref. [6]:

(i) Oscillating patterns in angular distributions can be observed in the following cases:

  (a) Resonance state is populated in transfer reaction on condition of "zero geometry" (e.g., Ref. [15]). The resonance state of interest is emitted at zero c.m. angle. Zero spin particles should take part in the population and decay of this state.
  (b) Sharp oscillating distributions can be observed in the case of direct reactions. Again, the state of interest should be populated and decay by zero spin particles. Correlations in such case are observed relative to the direction of momentum transfer.
  (c) To our knowledge, only one observation of oscillating pattern was reported for the $^{13}\mathrm{C}(^6\mathrm{Li}, d)^{17}\mathrm{O}^*(\alpha)^{13}\mathrm{C}_{\mathrm{g.s.}}$ reaction involving nuclei with nonzero spin [20]. It was shown in Ref. [21] that such observation can be explained only in the case that the energy degeneracy and interference of (at least) two states having different spins take place.

(ii) The ^{5}H system could be considered as a "proton hole" in ^{6}He (see, e.g., Ref. [9]). Theoretical predictions give $J^\pi = 1/2^+$ for the ground state of ^{5}H. The lowest excited

states are expected to be a doublet of the $3/2^+$ and $5/2^+$ states.

(iii) The ^{5}H g.s. is poorly populated in the two-neutron transfer reaction due to the statistical factor $(2J+1)$ and also as a consequence of the "angular momentum mismatch." The DWBA calculations substantiating this statement are presented in Sec. VI C.

(iv) The spin transfer is negligible. Spin transfer $\Delta S = 1$ is possible only if the two neutrons are in negative parity state of their relative motion. There is a broad experience of studies showing that the dineutron transfer ($\Delta S = 0$) is a much more favorable mode [22].

(v) To produce the strongly oscillating angular distributions it is necessary that the $3/2^+$ and $5/2^+$ states are degenerate or close to that. Theoretical calculations (e.g., Ref. [9]) show that the expected energy split between these states is much smaller than the widths of the states. So, this assumption looks reasonable.

(vi) To produce the strongly oscillating angular distributions it is necessary that the $\{L = 2, S_x = 0, l_x = 0, l_y = 2\}$ component of the wave function (WF) dominates in the decay of ^{5}H (L is the total angular momentum, subscripts x and y refer to the spins and angular momenta of the nn and $t-nn$ subsystems). This WF component corresponds to the d-wave motion of the triton in ^{5}H. This request matches with theoretical calculations made for ^{5}H [13] and ^{6}He [23] and with experimental results on the decay of the ^{6}He 2^+ state [24–29].

B. Theoretical formalism

The distribution of particles $p+t+n+n$ in the outgoing channel of the reaction is described by the following expression:

$$\frac{d^9N}{d\mathbf{k}_{nn}\,d\mathbf{k}_{t-nn}\,d\mathbf{k}_{^5\mathrm{H}-p}} \propto \sum_{\sigma} |F|^2\,\delta(E_{\mathrm{c.m.}} - E_{nn} - E_{t-nn} - E_{^5\mathrm{H}-p})\,, \qquad (1)$$

where $\mathbf{k}_{nn}$ is the relative momentum of the two neutrons, $\mathbf{k}_{t-nn}$ is the relative momentum of the triton and the center of mass of the two neutrons, $\mathbf{k}_{^5\mathrm{H}-p}$ is the relative momentum of the proton and the center of mass of the $t+2n$ system; E_{nn}, E_{t-nn}, and $E_{^5\mathrm{H}-p}$ are the corresponding relative energies. On the right side of Eq. (1), F is the reaction amplitude, the sum runs over unobserved projections of spins (denoted σ) of the particles, while the delta-function provides the energy conservation with $E_{\mathrm{c.m.}}$ being the total energy in the center of mass of outgoing channel. Equation (1) can be easily converted to

$$\frac{d^7N}{dE_{nn}\,d\Omega_{nn}\,dE_{^5\mathrm{H}}\,d\Omega_{t-nn}\sin(\theta_{^5\mathrm{H}-p})\,d\theta_{^5\mathrm{H}-p}} \propto \sqrt{E_{nn}(E_{^5\mathrm{H}} - E_{nn})(E_{\mathrm{c.m.}} - E_{^5\mathrm{H}})}\int \sum_{\sigma} |F|^2 d\varphi_{^5\mathrm{H}-p}, \qquad (2)$$

where $E_{^5\mathrm{H}} = E_{nn} + E_{t-nn}$.

In the analysis of $|F|^2$, we assume that the internal degrees of freedom for ^{5}H and the motion of ^{5}H as a whole are well factorized according to the two-step process which contains the ^{5}H formation stage and its decay stage. In this case the asymptotic part of the wave function of the $p+t+n+n$ system can be written as

$$\Psi^{(+)} = \sum_{J_tM_t} \left[\psi^{(+)}_{J_tJjm_j} \otimes \Psi^{(+)}_{JM}\right]_{J_tM_t}, \qquad (3)$$

where $\psi^{(+)}_{J_tJjm_j}$ is the wave function of relative motion in the $p+^5$H system and $\Psi^{(+)}_{JM}$ is the wave function of internal motion in the $t+n+n$ system. The "(+)" superscript indicates that we deal with the wave functions having only the outgoing asymptotic behavior. J and M are the total spin of the ^{5}H state and its projection; j and m_j describe the total angular momentum of the proton; J_t and M_t correspond to the total angular momentum in the outgoing $p+t+n+n$ channel.

The asymptotic form of the wave function of relative motion in the $p+^5$H system is

$$\psi^{(+)}_{J_tJjm_j}(E_{^5\mathrm{H}-p}, \hat{\mathbf{k}}_{^5\mathrm{H}-p}) = \frac{\exp[ik_{^5\mathrm{H}-p}r]}{r}\sum_l a^j_{J_tJl} \times [Y_{lm}(\hat{\mathbf{k}}_{^5\mathrm{H}-p}) \otimes \chi_{1/2\mu}]_{jm_j}, \qquad (4)$$

where $\chi_{1/2\mu}$ is the proton spin function.

The asymptotic form of the wave function of internal motion in the $t+n+n$ system is given by

$$\Psi^{(+)}_{JM}(E_{^5\mathrm{H}}, \Omega_5) = \frac{\exp[i\boldsymbol{\varkappa}\rho]}{\rho^{5/2}}\sum_{K\gamma} A^J_{K\gamma}(E_{^5\mathrm{H}})\,\mathcal{J}^{JM}_{K\gamma}(\Omega_5). \qquad (5)$$

This expression represents the expansion of the $t+n+n$ wave function in a hyperspherical harmonics series. Detailed definitions of the hyperspherical harmonics can be found, for example, in Ref. [30].

As a result, we obtain the following expression for the value

$$W \equiv \int \sum_{\sigma} |F|^2\, d\varphi_{^5\mathrm{H}-p}$$

from Eq. (2):

$$\begin{aligned} W = \sum_{J_tJ'_tM_t}\sum_{JJ'M}\sum_{jj'm_j}\sum_{ll'm\mu} & C^{J_tM_t}_{jm_jJM}C^{J'_tM_t}_{j'm_jJ'M}C^{jm_j}_{lm1/2\mu}C^{j'm_j}_{l'm1/2\mu} \\ & \times \left(a^j_{J_tJl}\right)^* a^{j'}_{J'_tJ'l'} N^m_l P^m_l(\cos\theta_{^5\mathrm{H}-p})\, N^m_{l'} P^m_{l'}(\cos\theta_{^5\mathrm{H}-p}) \\ & \times \sum_{SM_SS_x}\sum_{Kl_xl_y}\sum_{K'L'l'_xl'_y} C^{JM}_{LM_LSM_S}C^{J'M}_{L'M_LSM_S} \\ & \times \left(A^J_{KLSS_xl_xl_y}(E_{^5\mathrm{H}})\right)^* A^{J'}_{K'L'SS_xl'_xl'_y}(E_{^5\mathrm{H}}) \\ & \times \left(\mathcal{I}^{LM_L}_{Kl_xl_y}(\Omega_{\boldsymbol{\varkappa}})\right)^* \mathcal{I}^{L'M_L}_{K'l'_xl'_y}(\Omega_{\boldsymbol{\varkappa}}), \end{aligned} \qquad (6)$$

where $N^m_l P^m_l$ are the Legendre polynomials normalized to unity. In this equation, the last three lines correspond to the ^{5}H decay into $t+n+n$ in terms of the hyperspherical harmonics, while the first two lines contain information about the ^{3}H$(t, p)^5$H reaction details. For phenomenological treatment of the experimental data the information about the

^{3}H$(t, p)^5$H reaction was represented by the density matrix ρ for ^{5}H:

$$W \propto \sum_{JJ'M} \rho^{J'M}_{JM}(E_{^5\mathrm{H}-p}, \theta_{^5\mathrm{H}-p}) \sum_{SM_SS_x} \sum_{KLl_xl_y} \sum_{K'L'l'_xl'_y} \times C^{JM}_{LM_LSM_S} C^{J'M}_{L'M_LSM_S} \left(A^{J}_{KLSS_xl_xl_y}(E_{^5\mathrm{H}})\right)^* \times A^{J'}_{K'L'SS_xl'_xl'_y}(E_{^5\mathrm{H}}) \left(\mathcal{I}^{LM_L}_{Kl_xl_y}(\Omega_{\boldsymbol{\varkappa}})\right)^* \mathcal{I}^{L'M_L}_{K'l'_xl'_y}(\Omega_{\boldsymbol{\varkappa}}), \quad (7)$$

and the density matrix parameters were fitted to the experimental data.

C. Density matrix parametrization

In general, one could arbitrarily choose the Z axis in the c.m. system of ^{5}H and treat the ρ-matrix parameters as free in a fitting procedure. However, the proper choice of this axis and physical assumptions can reduce the number of free parameters. There are three physically selected directions in the experiment: The beam axis and the two directions of momentum transfer occurring in the ^{3}H(t, p) reaction. The availability of these two directions relates to the identity of the beam and target particles and corresponds to the dineutron transfer from the beam to the target triton and vice versa. The former direction ($\mathbf{q}_L = \mathbf{k}_{\mathrm{beam}} - \mathbf{k}_p$) corresponds to maximum cross section for fast protons moving in forward direction and coincides with the momentum of ^{5}H in lab system; the latter [$\mathbf{q}_{AL} = -(2/3)\mathbf{k}_{\mathrm{beam}} - \mathbf{k}_p$] corresponds to backward protons in lab system and coincides with the momentum of ^{5}H in the "antilaboratory" system (see Fig. 3). In Fig. 6 we present the angular distributions obtained for tritons in the ^{5}H c.m. system with respect to three quantization axes: $\mathbf{q}_L, \mathbf{k}_{\mathrm{beam}}$, and $-\mathbf{q}_{AL}$. Only events with $\varepsilon < 0.1$ (where the oscillations should be more pronounced) are shown in the picture. The difference between these axes is not too large as the mean angles between the beam axis and the $\mathbf{q}_L$ and $-\mathbf{q}_{AL}$ vectors are small (about -3° and $+5^\circ$, respectively). Nevertheless, there

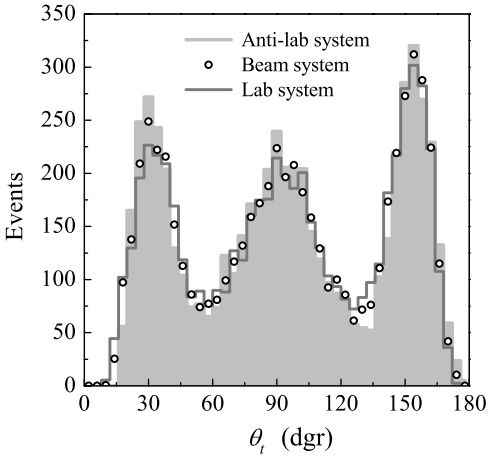

FIG. 6. Experimental distributions of events with $\varepsilon < 0.1$ over the angle θ_t obtained for different choices of the Z axis. Circles correspond to this axis chosen collinear with the beam axis, gray histogram—collinear with $\mathbf{q}_L$ ("lab system"), and filled histogram–collinear with $\mathbf{q}_{AL}$ ("antilab system"). See also Fig. 3 for details.

are statistically significant differences in the distributions, and one can clearly see these differences in Fig. 6. The maximal alignment (the maximal peak to dip ratio) corresponds to the dineutron transfer from the target triton to the beam triton [see Fig. 3(b)] and, hence, to the maximum of cross section at small c.m. angles of the ^{3}H(t, p) reaction (protons are emitted to the backward direction in the lab system). This observation enables us to treat the reaction leading to the population of ^{5}H resonances as a direct dineutron transfer (single pole graph approximation) from target to beam and to choose the Z axis along the $-\mathbf{q}_{AL} = (2/3)\mathbf{k}_{\mathrm{beam}} + \mathbf{k}_p$ vector. The reaction amplitude for the single pole graph mechanism should be axially symmetric (the so-called Treyman-Yang criterion).

In the case of the axial symmetry relative to the chosen quantization axis, the independent nonzero elements of the density matrix $\rho^{J'M}_{JM}$ for the $3/2^+ - 5/2^+$ doublet in ^{5}H can be parametrized by five parameters. We choose them as follows: r is the relative weight of the $5/2^+$ state in the $3/2^+ - 5/2^+$ doublet, c_{2J} are the relative weights of components with $M = \pm 1/2$ for the state with total momentum J, and $\phi^{(2|M|)}_{2J\,2J'}$ are the relative phases of components with J and J' with different M. In this parametrization the density matrix elements $\rho^{J'M}_{JM}$ are

$$\begin{aligned}
\rho^{3/23/2}_{3/23/2} &= \rho^{3/2-3/2}_{3/2-3/2} = (1-c_3)(1-r)/2,\\
\rho^{3/21/2}_{3/21/2} &= \rho^{3/2-1/2}_{3/2-1/2} = c_3(1-r)/2,\\
\rho^{5/23/2}_{5/23/2} &= \rho^{5/2-3/2}_{5/2-3/2} = (1-c_5)r/2,\\
\rho^{5/21/2}_{5/21/2} &= \rho^{5/2-1/2}_{5/2-1/2} = c_5 r/2,\\
\rho^{3/23/2}_{5/23/2} &= \left(\rho^{5/23/2}_{3/23/2}\right)^* = -\rho^{3/2-3/2}_{5/2-3/2} = -\left(\rho^{5/2-3/2}_{3/2-3/2}\right)^*\\
&= -\frac{\exp\left[i\phi^{(3)}_{35}\right]}{2}\sqrt{(1-c_3)(1-c_5)r(1-r)},\\
\rho^{3/21/2}_{5/21/2} &= \left(\rho^{5/21/2}_{3/21/2}\right)^* = -\rho^{3/2-1/2}_{5/2-1/2} = -\left(\rho^{5/2-1/2}_{3/2-1/2}\right)^*\\
&= -\frac{\exp\left[i\phi^{(1)}_{35}\right]}{2}\sqrt{c_3c_5r(1-r)}.
\end{aligned} \quad (8)$$

For the interference of the $3/2^+ - 5/2^+$ doublet with the $1/2^+$ state of ^{5}H, the matrix elements (8) should be supplemented with the following nonzero matrix elements:

$$\begin{aligned}
\rho^{1/21/2}_{1/21/2} &= \rho^{1/2-1/2}_{1/2-1/2} = w_1/2,\\
\rho^{1/21/2}_{3/21/2} &= \left(\rho^{3/21/2}_{1/21/2}\right)^* = -\rho^{1/2-1/2}_{3/2-1/2} = -\left(\rho^{3/2-1/2}_{1/2-1/2}\right)^*\\
&= -\frac{\exp[i\phi_1]}{2}\sqrt{w_1c_3(1-r)},\\
\rho^{1/21/2}_{5/21/2} &= \left(\rho^{5/21/2}_{1/21/2}\right)^* = -\rho^{1/2-1/2}_{5/2-1/2} = -\left(\rho^{5/2-1/2}_{1/2-1/2}\right)^*\\
&= -\frac{\exp\left[i\left(\phi_1+\phi^{(1)}_{35}\right)\right]}{2}\sqrt{w_1c_5r},
\end{aligned} \quad (9)$$

where w_1 is the weight of $1/2^+$ state relative to the $3/2^+ - 5/2^+$ doublet. The ρ-matrix should also be renormalized according to $Sp[\rho] = 1$.

The above parametrizations are assumed to be independent of the energy $E_{^5\mathrm{H}-p} = E_{\mathrm{c.m.}} - E_{^5\mathrm{H}}$ (the only exception will be the phase ϕ_1 of the $1/2^+$ state), and dependence on the

energy $E_{^5\mathrm{H}}$ will be included in the parametrization of decay amplitudes $A^J_{K\gamma}$.

D. Qualitative discussion of correlations

In the case of the $3/2^+ - 5/2^+$ doublet degeneracy, we can consider that the amplitudes $A^J_{KLSS_xl_xl_y}$ in Eq. (7) do not depend on total angular momentum J and that the correlations are described by a density matrix, which depends on the total orbital angular momentum L

$$\rho^{L'M_L}_{LM_L} = \sum_{JJ'M}\sum_{M_S} C^{JM}_{LM_LSM_S} C^{J'M}_{L'M_LSM_S}\,\rho^{J'M}_{JM}. \qquad (10)$$

The relative phases $\phi^{(1)}_{35}$ and $\phi^{(3)}_{35}$ should be taken to be zero in this case. For parametrization (8) the nonzero elements of the density matrix (10) with $S = 1/2$ and for the summary spin of the two neutrons $S_x = 0$ are

$$\begin{aligned}
\rho^{20}_{20} &= \tfrac{1}{5}\big[2(1-r)c_3 + 3\,rc_5 + 2\sqrt{6c_3c_5r(1-r)}\big],\\
\rho^{21}_{21} &= \rho^{2-1}_{2-1} = \tfrac{1}{10}\big[1 + 3r + 2(1-r)c_3 - 2rc_5\\
&\quad + 4\sqrt{(1-c_3)(1-c_5)r(1-r)} - 2\sqrt{6c_3c_5r(1-r)}\big],\\
\rho^{22}_{22} &= \rho^{2-2}_{2-2} = \tfrac{1}{10}\big[4(1-r)(1-c_3) + r(1-c_5)\\
&\quad - 4\sqrt{(1-c_3)(1-c_5)r(1-r)}\big]. \qquad (11)
\end{aligned}$$

If we assume only one $\{LS_xl_xl_y\} = \{2002\}$ component in ^{5}H, the inclusive correlation spectrum over the angle θ_t can be represented as

$$\frac{dW}{d\theta_t} \propto \sum_{M_L=-2}^{2} \rho^{2M_L}_{2M_L}\big[P_2^{M_L}(\cos\theta_t)\big]^2 \sin\theta_t. \qquad (12)$$

If the reaction corresponds to zero spin transfer, then the alignment of the ^{5}H states is complete, and the coefficients c_3 and c_5 should be taken as unity. Indeed, the total momentum projections $M = \pm 3/2,\ \pm 5/2$ cannot be populated in such case for zero geometry (or direct reaction). This leads to $\rho^{22}_{22} = 0$. After that, condition can be obtained, under which $\rho^{21}_{21} = 0$. This is $r = 3/5$, which is just the combinatorial value for the $3/2^+$ and $5/2^+$ states, and it can also be easily inferred from the total momentum degeneracy.

So, the assumptions of zero angle geometry (direct character of reaction), the degeneracy of the $3/2^+$ and $5/2^+$ states, and the $\Delta S = 0$ transfer lead to a parameter free density matrix. Under the assumption of Eq. (12) this results in the correlation function

$$\frac{dW}{d\theta_t} \propto \big[P_2^0(\cos\theta_t)\big]^2 \sin\theta_t. \qquad (13)$$

It is clear that, already in the first approximation, this simple picture provided by evident physical assumptions qualitatively describes the main features of the experimental data (see Fig. 4).

The behavior of the θ_t angular correlation in the above chosen case of one component in the ^{5}H WF, but in situations of more general mixing between $3/2^+$ and $5/2^+$ states, is illustrated in Figs. 7 and 8. The following aspects of the distributions should be emphasized:

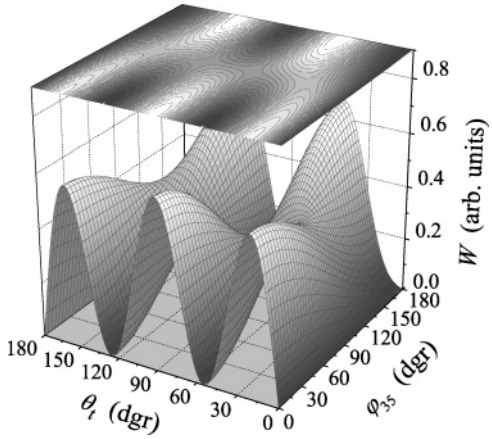

FIG. 7. Distribution over the angle θ_t for the interference of the $3/2^+$ and $5/2^+$ states as a function of phase $\phi^{(1)}_{35}$. The calculation was made for the case of complete alignment, one $\{LS_xl_xl_y\} = \{2002\}$ component, and $r = 3/5$.

(i) The picture with three strong peaks is not necessarily expected in general case: over the broad ranges of parameter space, qualitatively different distributions are obtained.

(ii) In the case of pure $3/2^+$ ($r = 0$) or pure $5/2^+$ ($r = 1$) the sharp oscillating pattern is not formed. In these cases there are two or three small peaks on a large background. A considerable mixing of states with different J is required to get sharp oscillations.

(iii) In the case of triple-peak correlation all three peaks have approximately the same heights. Any variation of the ρ-matrix parameters does not allow one to vary considerably the ratio of the peak heights.

The angular distribution over θ_t (Fig. 4) is stable above 2.5 MeV; below this value the peak at $\theta_t = 90^\circ$ is enhanced. We have found that the only physically justified way to enhance strongly the central peak ($\theta_t = 90^\circ$) is to mix the $3/2^+ - 5/2^+$

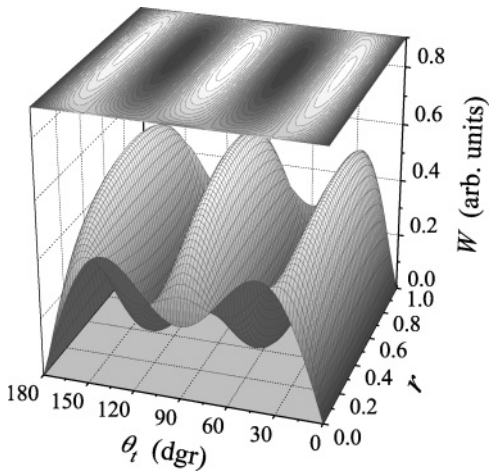

FIG. 8. Distribution over the angle θ_t for the interference of the $3/2^+$ and $5/2^+$ states as a function of the $5/2^+$ to $3/2^+$ ratio r. The calculation was made for the case of complete alignment, one $\{LS_xl_xl_y\} = \{2002\}$ component, and $\phi^{(1)}_{35} = 0$.

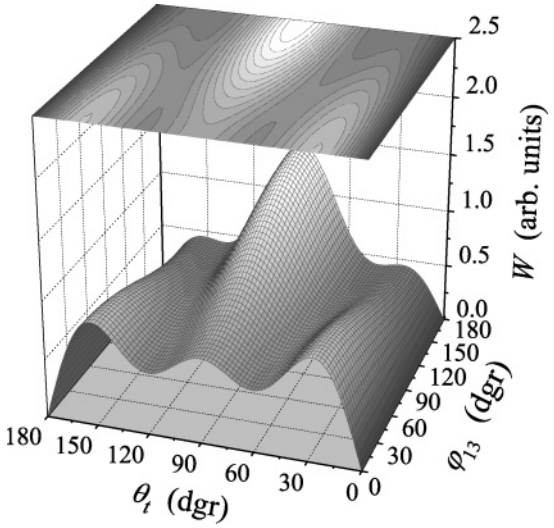

FIG. 9. Distribution over the angle θ_t for the interference of the $1/2^+$ g.s. with the mixture of the $3/2^+$ and $5/2^+$ states as a function of phase ϕ_{13}. The $3/2^+$ and $5/2^+$ mixture is fitted to the experimental data at $E_{^5\mathrm{H}} \sim 4.5$ MeV. The fraction of the $1/2^+$ admixture is $w_1 = 0.7$.

doublet with the $1/2^+$ state. In this case the valleys between peaks become less pronounced, but the central peak can be much larger than the satellites. An example of angular distribution dependence on the mixing parameters is given in Fig. 9 for one selected case of the $1/2^+/(3/2^+ - 5/2^+)$ ratio. The contribution of the ground state of ^{5}H in the low-energy range can be deduced from this analysis.

V. DATA ANALYSIS PROCEDURE

In our analysis of the data we assumed that the amplitudes are factorized [see Eq. (7)] into products of terms corresponding to the internal motion of ^{5}H ($A^J_{K\gamma}$) and terms corresponding to the motion of ^{5}H states as a whole (described by the ρ-matrix). The analysis has been performed in the assumption of complete degeneracy for the $3/2^+$ and $5/2^+$ doublet and population of minimal magnetic substates (see also Sec. VI A). This leaves only w_1 and $\phi^{(1)}_1$ in Eqs. (8) and (9) as free parameters. The relative weight of the $3/2^+$ and $5/2^+$ states is fixed by the vector coupling coefficients to be $r = 3/5$, c_3 and c_5 should be taken as unity, and the relative phases $\phi^{(1)}_{35}$ and $\phi^{(3)}_{35}$ should be taken as zero.

Experimental details (geometry, detection efficiency and thresholds, beam and target parameters, energy and time resolution, etc.) were taken into account by Monte Carlo simulation. Due to a very complicated efficiency correction the direct χ-square procedure is not applicable to the present data analysis. Instead, the fitting procedure was done iteratively with three steps at each iteration:

(i) The internal E_{nn} distribution is fitted within definite $E_{^5\mathrm{H}}$ bins. The coefficients of the expansion over hyperspherical harmonics are extracted.
(ii) Then the angular distributions in the ^{5}H frame (again within definite $E_{^5\mathrm{H}}$ bins) are fitted. Parameters of the ρ-matrix are extracted.
(iii) Combining all the $E_{^5\mathrm{H}}$ bins, the profile of the ^{5}H spectrum $E_{^5\mathrm{H}}$ is fixed.

A. Internal energy distribution for ^{5}H

Amplitudes $A^J_{K\gamma}$ were parametrized as products of slowly and rapidly changing terms:

$$A^J_{K\gamma} = a^J_{K\gamma}(E_{^5\mathrm{H}})\ f_J(E_{^5\mathrm{H}}); \quad \sum_{K\gamma} \left|a^J_{K\gamma}(E_{^5\mathrm{H}})\right|^2 = 1. \quad (14)$$

The amplitudes were assumed to be the same for the $3/2^+$ and $5/2^+$ states. For the $1/2^+$ state, the energy dependence of the amplitudes $a^J_{K\gamma}(E_{^5\mathrm{H}})$ was neglected. As it was not possible to disentangle the contributions of the $1/2^+$ state and the $3/2^+ - 5/2^+$ pair in the low energy region, coefficients $a^{1/2}_{K\gamma}$ were chosen to give the same E_{nn} distribution as the $3/2^+ - 5/2^+$ doublet. Coefficients $a^{3/2,5/2}_{K\gamma}$ were fitted within several $E_{^5\mathrm{H}}$ bins. They are provided in Table I. For MC simulation the coefficients were linearly interpolated between the provided values; beyond the range of Table I they were taken as constant. The quality of the fit for the distributions over E_{nn} can be seen in Fig. 10.

Energy distributions provided by the coefficients from Table I are shown in Fig. 11 for some energies $E_{^5\mathrm{H}}$. These

TABLE I. Hypersperical decompositions of decay amplitudes $a^J_{K\gamma}$; coefficients are multiplied by a factor of 100. The weights of different components are given for the ground state at $E_{^5\mathrm{H}} = 2$ MeV and for the excited doublet at $E_{^5\mathrm{H}} = 5$ MeV.

$E_{^5\mathrm{H}}$ (MeV)														Weight
J	K	L	l_x	l_y	S_x	2		3		4		5		(%)
						Re [a]	Im [a]	Re [a]	Im [a]	Re [a]	Im [a]	Re [a]	Im [a]	
3/2, 5/2	2	2	2	0	0	−48.26	0	−47.25	0	−48.61	0	−47.32	0	22.4
	2	2	0	2	0	82.45	0	79.32	0	76.29	0	72.93	0	53.2
	4	2	0	2	0	7.65	5.26	16.18	15.06	24.28	18.11	29.21	22.45	13.6
	6	2	0	2	0	10.39	26.06	7.58	30.48	3.95	29.73	3.53	32.74	10.8
1/2	0	0	0	0	0	95.78	0	95.78	0	95.78	0	95.78	0	91.7
	2	0	0	0	0	20.03	0	20.03	0	20.03	0	20.03	0	4.0
	4	0	0	0	0	19.48	0	19.48	0	19.48	0	19.48	0	3.8
	6	0	0	0	0	6.78	0	6.78	0	6.78	0	6.78	0	0.5

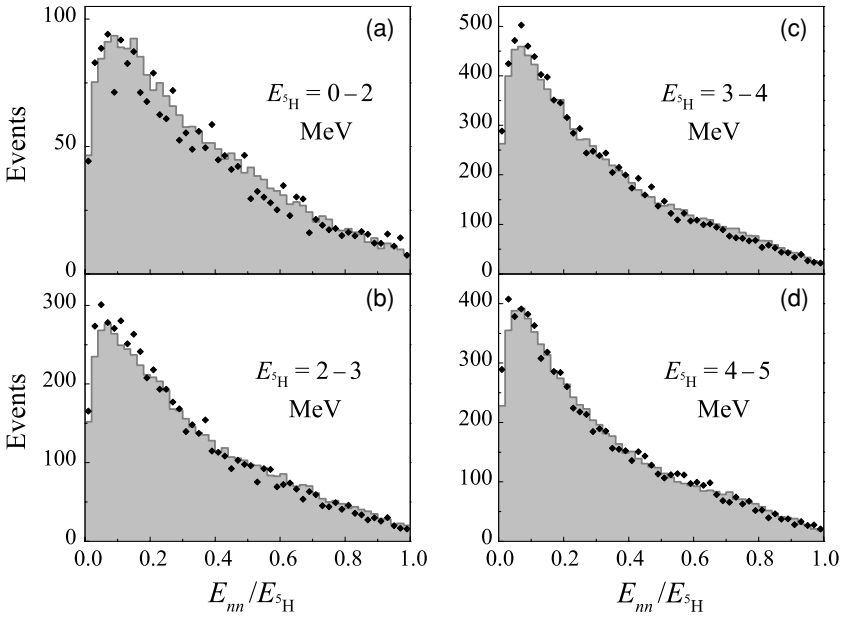

FIG. 10. Relative energy spectrum for two neutrons in ^{5}H for different $E_{^5H}$ energy bins. Panels (a), (b), (c), and (d) correspond to the 0–2, 2–3, 3–4, and 4–5 MeV bins, respectively. Diamonds show the data, and the gray histograms are the results of MC simulation.

distributions are used as input for the MC simulation and can be considered as efficiency corrected spectra. They demonstrate quite a systematic evolution with ^{5}H energy. This is also reflected by the relatively weak dependence of the hyperspherical coefficients on energy. An interesting feature of these distributions is the behavior of dineutron peak, which becomes relatively narrower as $E_{^5H}$ increases (see Fig. 10). However, when plotted as a function of real energy E_{nn}, the width of this peak slowly grows and seems to be reasonably consistent with the case of "bare" n-n interaction only for $E_{^5H} \sim 5$ MeV. The latter is given by a Migdal-Watson type expression,

$$\frac{dW}{dE_{nn}} \sim \frac{\sin^2 \delta_0(E_{nn})}{\sqrt{E_{nn}}},$$

not limited in the sense of maximal n-n energy (see Fig. 11, gray curve). A narrow (compared to Migdal-Watson)

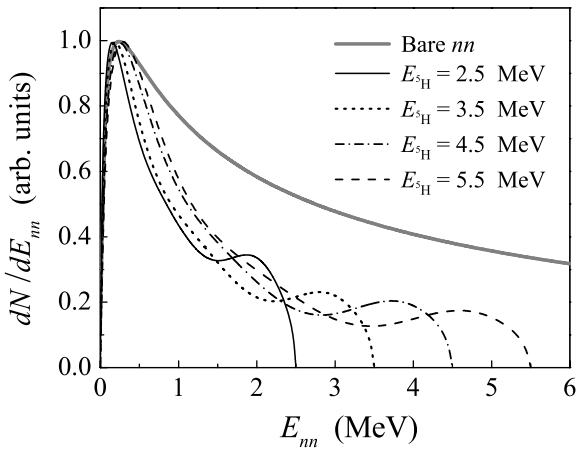

FIG. 11. Evolution of the reconstructed (corrected for efficiency) E_{nn} distribution with energy $E_{^5H}$, and scaling of the n-n peak with energy. The gray curve corresponds to "bare" case of final state n-n interaction.

dineutron peak is the feature of $2n$ decays, which have already been noted (see, e.g., Refs. [25,27]).

The hyperspherical decomposition of the decay amplitude in Table I provides, on one hand, a compact and complete representation of the experimental data. On the other hand, this decomposition reflects the dynamics of the decay. Namely, the dominant weights of the components with the lowest values of hypermomentum K correspond to the lowest three-body centrifugal barrier, and such large weights for minimal K values are expected from theoretical calculations. As for the higher order terms in Table I, having small weights, they should not be straightforwardly compared with results presented by theoretical calculations, because a truncated hyperspherical basis has been obviously used in order to fit the experimental data.

Complete description of the internal motion of a three-body system with a given total energy can be done using two variables. Together with variable $E_{nn}/E_{^5H}$, describing the energy distribution between the subsystems, it is convenient to use the angle between the Jacobi momenta

$$\cos(\theta_k) = (\hat{k}_{nn}, \hat{k}_{t-nn}). \tag{15}$$

The distributions over this variable are shown in Fig. 12 for different energy bins. The dependence of this distribution on energy is not significant. The angular dependence considered at fixed energy values $E_{^5H}$ is relatively weak: The T-like configuration of outgoing particles ($\theta_k \sim 90^\circ$) is somewhat more preferable than the linear configuration ($\theta_k \sim 0^\circ$). Such features of this angular distribution have been already observed in Ref. [4].

B. Angular correlations in the ^{5}H c.m. frame

Figure 13 demonstrates the quality of the fit to the data with and without taking the ground state into account. The population of the doublet of excited states describes well the data above 2.5 MeV with no free parameters in the ρ-matrix [Fig. 13(c)]. Below 2.5 MeV the enhancement of

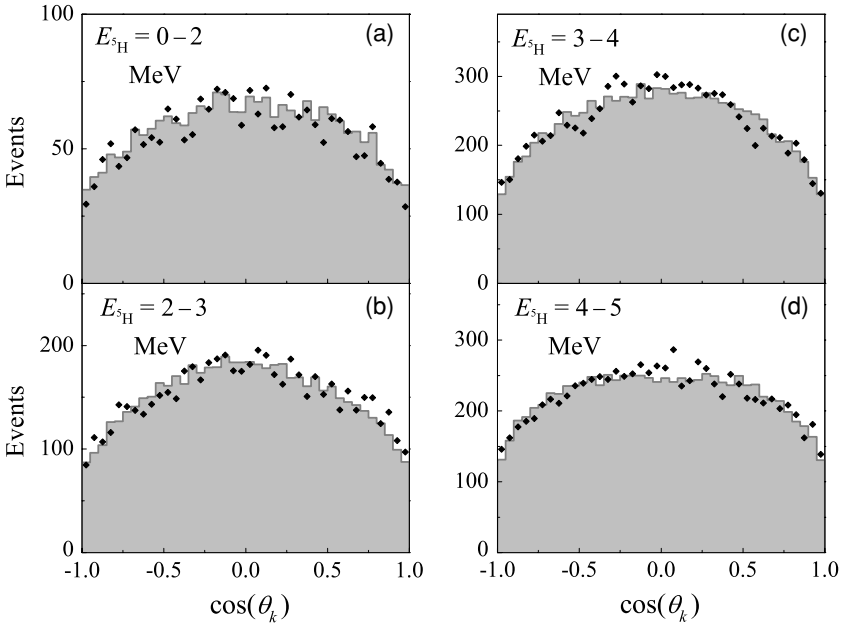

FIG. 12. Distribution of particles in ^{5}H as a function of the cosine of the angle θ_k between the relative momenta $\mathbf{k}_{nn}$ and $\mathbf{k}_{t-nn}$ [see Eq. (15)] for different $E_{^5\mathrm{H}}$ energy bins. Panels (a), (b), (c), and (d) correspond to $0-2$, 2–3, 3–4, and 4–5 MeV bins, respectively. (See notations in caption to Fig. 10.)

the central peak cannot be fitted under this assumptions. A natural suggestion of the population of the $1/2^+$ ground state drastically improves the situation [see Fig. 13(b)]. The energy dependence of the ground state phase ϕ_1 was approximated using the R-matrix expression for phase shift in the vicinity of a resonance

$$\phi_1 = \frac{\pi}{2} + \arctan\left(\frac{\Gamma_{\mathrm{g.s.}}}{2(E_{\mathrm{g.s.}} - E_{^5\mathrm{H}})}\right),$$

where $E_{\mathrm{g.s.}} = 1.8$ MeV and $\Gamma_{\mathrm{g.s.}} = 1.3$ MeV.

Energy profiles f_J are presented in Table II. Figures 14 and 15 demonstrate the quality of the fits to the triton and neutron angular distributions (respectively) in different bins of the ^{5}H missing mass spectrum. The efficiency corrected distributions extracted from the data are shown in Fig. 16.

C. Missing mass spectrum of ^{5}H

The missing mass spectrum of ^{5}H is shown in the lower panel of Fig. 17 together with the results of a MC simulation. In the upper panel of Fig. 17 the reconstructed spectrum (corrected for efficiency) and contributions of different states are shown.

TABLE II. Energy profiles f_J of different states in ^{5}H.

$E_{^5\mathrm{H}}$ (MeV)	$f_{1/2}$	$f_{3/2,5/2}$	$E_{^5\mathrm{H}}$ (MeV)	$f_{1/2}$	$f_{3/2,5/2}$
0.25	0.0276	0.0316	2.5	0.486	1.45
0.5	0.0781	0.0707	2.75	0.437	1.64
0.75	0.160	0.224	3.0	0.400	1.80
1.0	0.268	0.316	3.5	0.376	2.11
1.25	0.388	0.500	4.0	0.338	2.35
1.5	0.532	0.632	4.5	0.315	2.50
1.75	0.611	0.806	5.0	0.300	2.54
2.0	0.608	1.02	5.5	0.283	2.57
2.25	0.545	1.24			

In the high energy part, the spectrum differs considerably from the reconstructed spectrum given in Ref. [6]. This is connected with some improvements made in this work for the efficiency treatment. The updated missing mass spectrum seems to achieve the "saturation": The peak energy is either achieved in the vicinity of 5 MeV or is close to that. We do not see the right slope of the excited states peak and cannot make a reliable quantitative statement on this question. A peak energy of 5 MeV or slightly higher looks reasonable.

VI. DISCUSSION

A. General notes

(i) We would like to emphasize once again that correlations observed in the present experiment could arise only under very specific conditions. Still many of these conditions can be satisfied by a proper choice of the reaction and experimental setup. Therefore the method proposed in the present work could be adapted for other studies.

(ii) As it was mentioned above the experimental data represent the six-dimensional array of independent variables showing rather strong correlations. Only the most representative projections of the data are shown and discussed in the paper. Nevertheless, we should note here that the overall agreement in description of distributions of *any* variables and their correlations has the same quality as those illustrated in Figs. 10, 12, 14, 15, and 17.

(iii) The weight of the WF component with the spin of two neutrons $S_x = 1$ (or in more detailed form $\{LS_xl_xl_y\} = \{2111\}$) was found to be consistent with zero in this analysis. This prescription was done due to a rapid degradation of agreement in Figs. 15(c) and 15(d) for the weight of this configuration exceeding some percent. An analogous WF component in ^{6}He is known to have weight around 15%. Comparable weights of this component are predicted in the theoretical calculations of ^{5}H. The absence of this component in the data can be connected

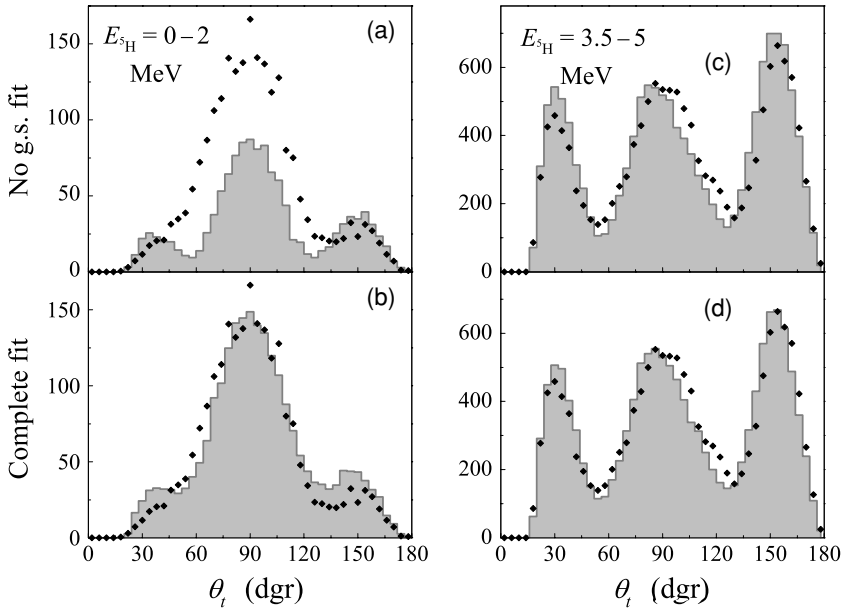

FIG. 13. Distribution over the angle θ_t in ^{5}H for $E_{^5H} < 2$ MeV (left column) and $E_{^5H} > 3.5$ MeV (right column). The two rows correspond to the fits *without* (a), (c) and *with* (b), (d) the ground state contributions. (See notations in caption to Fig. 10.)

with the small lifetime of ^{5}H and specific reaction mechanism (presumably direct *nn* transfer with $\Delta S = 0$).

(iv) In the provided fit to the data the population of higher magnetic substates in the ρ-matrix was neglected. It was found that some admixture (but not more than ~10%) of such substates is possible; however, it does not improve the agreement with data.

(v) Theoretical ansatz suggested in Sec. IV and the data analysis procedure described above provide an excellent fit to the data. Thus, we may conclude unambiguously that the $3/2^+ - 5/2^+$ doublet is predominantly populated in this reaction, and these two states are energy degenerate or close to that. Even if we cannot quote precise values for the peak position and width, the analysis shows that the observed missing mass spectrum (practically) reaches its maximum value (see Fig. 17).

(vi) The complete missing mass spectrum for ^{5}H itself is smooth and does not show any evidence for the ground state. However, the angular correlations could not be reproduced without assuming the presence of a $1/2^+$ state at about 1.8 MeV. This description may not be unique, but we were not able to find consistent alternative explanation for all available facts. At that point a comparison with the first ^{3}H(t, p) experiment [3] and more detailed look in the missing mass spectrum of this work may be helpful.

B. Comparison with the previous ^{3}H(t, p) experiment

The first study of the ^{3}H(t, p)^{5}H reaction [3] was performed at the same beam energy as here, but with different kinematical conditions. The recoil protons were registered in a forward direction in the lab system. This resulted in a significantly broader range of measured ^{5}H energies, but the reaction

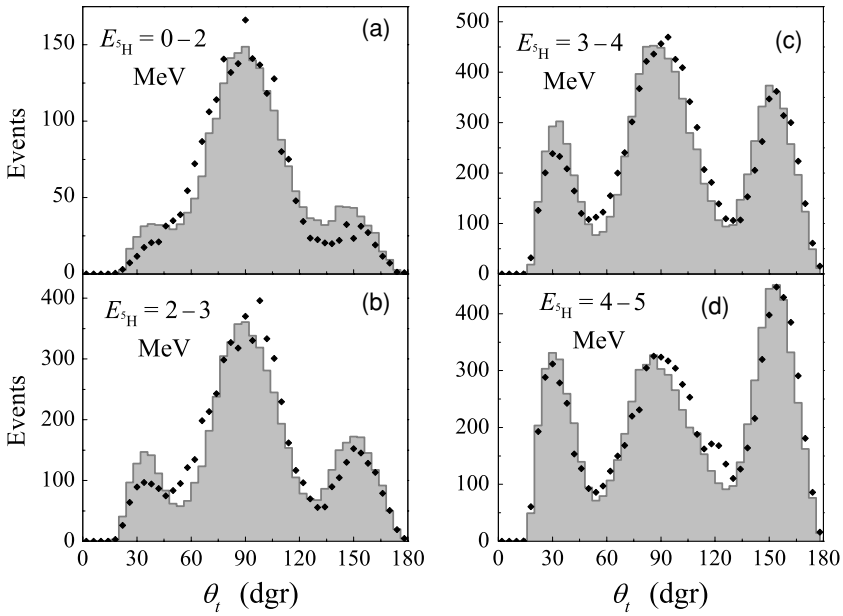

FIG. 14. Distribution over the angle θ_t in ^{5}H for different $E_{^5H}$ energy bins. Panels (a), (b), (c), and (d), correspond to 0–2, 2–3, 3–4, and 4–5 MeV bins, respectively. (See notations in caption to Fig. 10.)

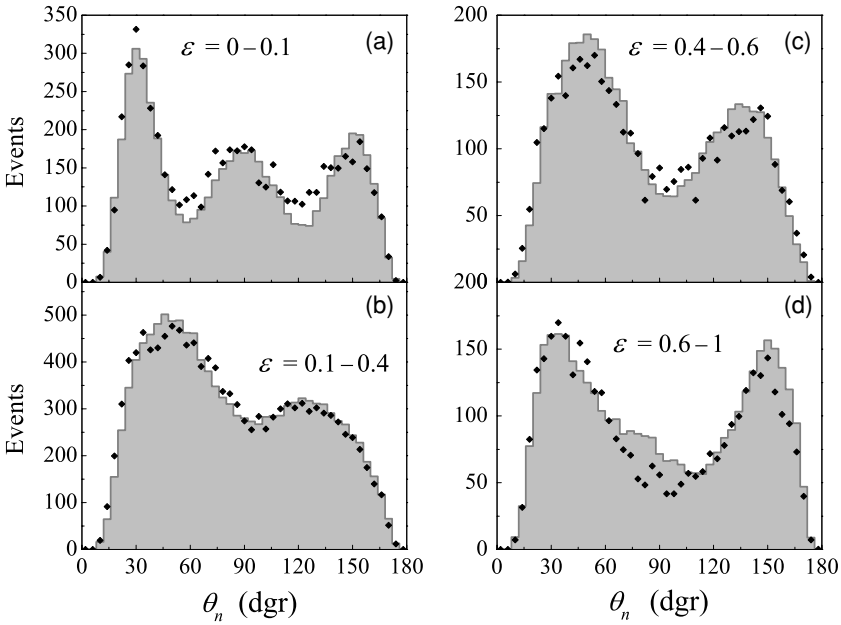

FIG. 15. Distribution over the angle θ_n in ^{5}H for different bins in $\varepsilon = E_{nn}/E_{^5\mathrm{H}}$. Panels (a), (b), (c), and (d) correspond to 0–0.1, 0.1–0.4, 0.4–0.6, and 0.6–1 bins, respectively. (See notations in caption to Fig. 10.)

mechanism was difficult to identify. A peak with a small width [$\Gamma \sim 0.5$ MeV, see Fig. 18(c)] was observed at 1.8 MeV. Such a low width is unexpected in theoretical models. It was suggested that the width of the peak could be due to the interference of the ^{5}H ground state with other continuum states.

In fact, for missing mass spectra one would expect that the contributions of states with different J^π add up incoherently. Integration over the whole angular range should provide orthogonality for different J^π. In the previous experiment [3] the missing mass spectrum was constructed using coincidences of decay products registered in a limited angular range. This means that orthogonality is not provided and that states with different J^π may interfere. In the present experiment the registration of ^{5}H decay products was provided in a much broader angular range. This reduced the interference effects in the missing mass spectrum drastically (see Fig. 17).

The missing mass spectra of ^{5}H are shown in Figs. 18(a) and 18(b) for two different bins in θ_t(lab). This figure illustrates the appearance of sharp interference patterns at the resonance position when the experimental acceptance is limited. The same spectrum, plotted for the whole range of accessible angles, is smooth around 1.8 MeV (Fig. 17). The cuts were chosen to enhance the rapid energy dependence around the expected energy of the ground state. The spectrum shown in Fig. 18(b) is consistent with the spectrum from Ref. [3], reproduced also in Fig. 18(c). Figure 18(a) shows that the spectrum obtained for different angular conditions may present a dip instead of a peak at this energy. The MC simulation

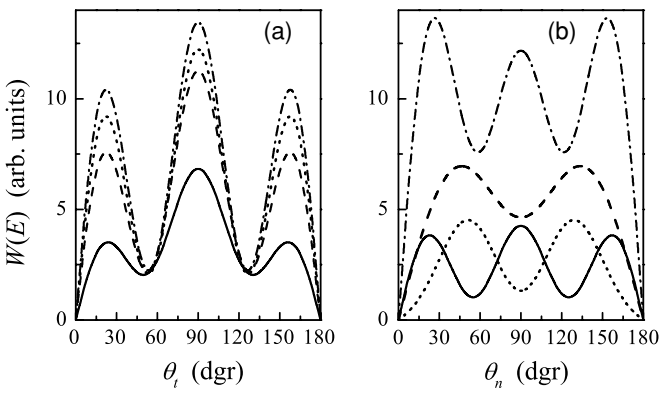

FIG. 16. Reconstructed efficiency corrected distributions over the angles θ_t [panel (a)] and θ_n [panel (b)]. The solid, dashed, dotted, and dash dotted curves correspond to panels (a), (b), (c), and (d) in Figs. 14 and 15.

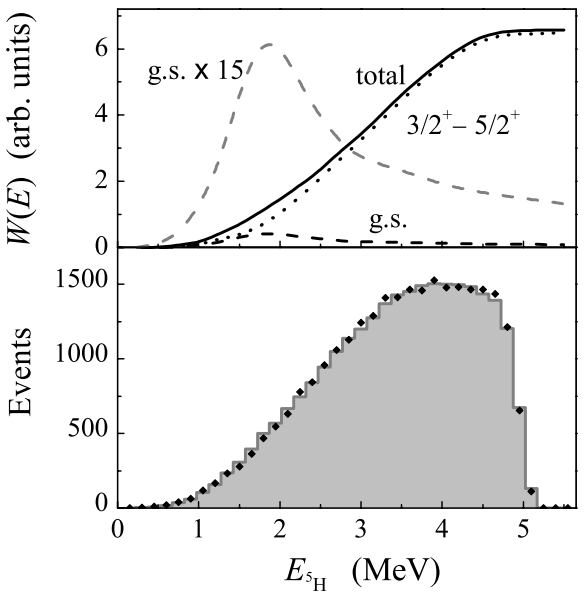

FIG. 17. Upper panel: The reconstructed missing mass spectrum of ^{5}H, corrected for efficiency. The solid curve is the result of the fit (the input for MC simulation). The dashed and dotted curves show the contributions of the $1/2^+$ state and $3/2^+$, $5/2^+$ mixture, respectively. Lower panel: The experimental missing mass spectrum of ^{5}H. (See notations in caption to Fig. 10.)

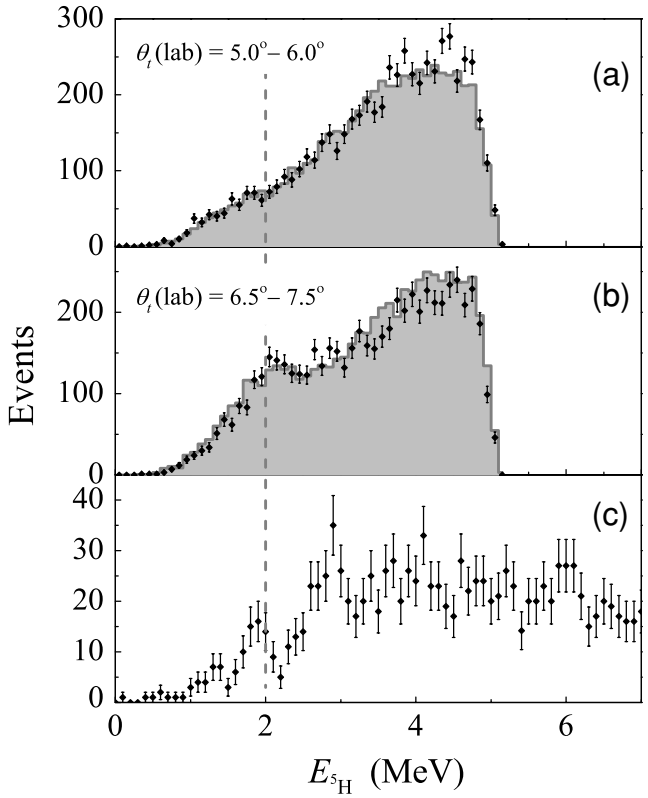

FIG. 18. Panels (a), (b) show the missing mass spectra of ^{5}H obtained in the present work for the two different ranges of the angle θ_t taken in laboratory frame. Panel (c) shows the spectrum of ^{5}H obtained in Ref. [3]. (See notations in caption to Fig. 10.)

nicely reproduces the peculiarities of the interference patterns in Figs. 18(a) and 18(b). So, the result of the present and previous experiments are comparable, the narrow structures found for some angular conditions are connected presumably with interference conditions, and the energy at which they are observed is consistent with the quoted position of the ground state of ^{5}H.

C. Discussion of DWBA calculations

In Ref. [6] the suppression of the ground state population in the ^{3}H(t, p)^{5}H reaction was explained qualitatively using the "angular momentum mismatch" argument. This is a quasiclassical speculation telling that, if one assumes that the dineutron transfer takes place at a given impact parameter, then the light proton cannot carry out of the system as much angular momentum as the heavier triton projectile brings in. For that reason $\Delta L = 0$, and hence the ground state population is suppressed as compared to the excited states population. DWBA calculations (see Appendix) confirm this idea. The behavior of the cross section dependence shown in Fig. 20 illustrates the "angular momentum mismatch" property, showing a strong peak at a nonzero transferred momentum ($\Delta L = 3$).

We draw also two important conclusions from these results:

(i) The ground state population ($\Delta L = 0$ transition) has a strong maximum at forward angles. However, even in the range of small angles it is strongly suppressed compared to the transition into the excited states ($\Delta L = 2$). The calculated ratio $\sigma_2/\sigma_0 = 44$ corresponds well to the population ratio, which was estimated from the experimental data to be around 30 ($\sigma_0 = 150 \pm 50$ μb/sr and $\sigma_2 = 4.6 \pm 2$ mb/sr, see also Fig. 17).

(ii) The DWBA calculations are nonspecific in the sense that they do not imply that one state in ^{5}H continuum is more preferable than another. We see from Fig. 20 that states with $\Delta L = 2$–6 are well populated in this model. This means that the strong population of states in ^{5}H with $\Delta L = 2$, observed in this experiment, cannot be a kind of "kinematical" effect connected only with peculiarities of the reaction mechanism, but should have its origin in the dynamics of the ^{5}H system, enhancing some particular set of quantum numbers.

D. Other experimental results

The idea to observe spin alignment in the decay of the three-body states with total angular momentum $J > 1/2$ is not new. A formalism for the analysis of decay data in the case of spin alignment was presented in Ref. [31]. Some evidence for spin alignment in the decay of the ^{6}He 2^+ state was obtained in Ref. [27]. A triple peak angular distribution of α particles coming from the decay of the 2^+ state in ^{6}He was reported in Ref. [32]. The 2^+ state of ^{6}He in this case was populated in a high-energy nuclear excitation reaction.

Important difference between the present results and the mentioned works is that (i) we deal with a system of half integer spin and (ii) we do not study alignment results for a system of known spin, but infer the spin of a system assuming alignment. Thus our work somehow "finalizes" the efforts of the mentioned previous works, and for the first time it demonstrates that quantitative results of significant interest can really be extracted from data connected with the spin alignment of a three-body system.

The ^{5}H system has been studied in several experiments providing sometimes contradictory results. The g.s. of ^{5}H was observed at $E_{^5\mathrm{H}} = 1.7(3)$ MeV with $\Gamma = 1.9(4)$ MeV in the proton pickup reaction ^{6}He(p,^{2}He)^{5}H [2]. It is expected that, due to similarities in the structure of ^{6}He and ^{5}H, the ground state of ^{5}H is predominantly populated in this reaction. From the measured angular distribution of the diproton center-of-mass evidence was inferred in Ref. [2] that $\Delta L = 0$ was really dominating in this reaction. The result of the present work concerning the ^{5}H g.s. energy is in agreement with Ref. [2]. Next to the ground state peak, a broad structure was observed in Ref. [2] with a maximum at about 5 MeV. The right-hand slope of this structure was formed by the decrease of efficiency. So, the peak position of this structure, seen in the ^{5}H spectrum presented in Ref. [2], is not evident. However, the mere fact that such a structure, lying in this energy range, was observed in the ^{6}He(p,^{2}He)^{5}H reaction is consistent with the results of our current studies.

Meister *et al.* [4] studied the ^{5}H continuum populated in the reaction of high-energy proton knockout from ^{6}He on a carbon target. A broad structure was observed, with a maximum at $E_{^5\mathrm{H}} = 3$ MeV and typical width around 6 MeV. Due to the presumable structure similarities between ^{6}He and ^{5}H, the

population of the g.s. of ^{5}H was expected to be dominant also in this case. Moreover, $\Delta L = 0$ is a typical feature for this class of reactions. This statement is, however, not proved experimentally. Theoretical estimates [14] show that the ^{5}H spectrum observed in this work can be explained assuming some contribution of excited states. It was also shown in Ref. [14] that the picture of *internal* correlations for ^{5}H, obtained in Ref. [4] does not contradict the population of excited states. The results of our work confirm that the internal correlations do not change drastically, when we compare energy regions, where the contribution of the ground state is important, and where there are only excited states [e.g., compare panels (a) and (d) in Figs. 10 and 12]. So, at least in the ^{5}H case, the internal correlations only cannot provide a clear evidence for the angular momentum of the state.

In the pion absorption reaction ^{9}Be(π^-, pt/dd)^{5}H, which was employed in Ref. [5], one should not expect any angular momentum selectivity, and all the low-lying states could be present in the experimental data. In this experiment, the first peak in the missing mass spectrum of ^{5}H was observed at $E_{^5\mathrm{H}} = 5.5$ MeV with $\Gamma = 5.4$ MeV. Angular momentum identification or correlation measurements were not made in this work. It is not impossible that the first peak, was actually formed by a broad overlap of the excited states in ^{5}H. Then the ground state could be "lost" in the slope of the well populated excited states, as it happened in the missing mass spectrum reported in the present work (see Fig. 17).

VII. CONCLUSION

In this work we have studied the continuum of the ^{5}H nucleus up to 5 MeV of c.m. energy. It was populated in the ^{3}H(t, p)^{5}H transfer reaction using a 57.7 MeV triton beam. The complete kinematics of the reaction has been provided. Efficiency corrections have been made utilizing the full information about the correlations of particles emitted in this reaction. The results have been presented in analytical form giving possibility for a straightforward comparison with theory.

The energy spectrum of ^{5}H obtained in this experiment is quite featureless. However, a deep insight in the data structure was possible due to the high statistics. A complicated correlation picture, varying with the ^{5}H energy, has been observed in this reaction. It was explained in the present work by several structural and dynamical factors: (i) comparatively small c.m. angles of the outgoing ^{5}H, (ii) direct one step character of the reaction in the chosen kinematical conditions, (iii) domination of dineutron transfer and hence $\Delta S = 0$ in this reaction, (iv) population of both the ground and excited states of ^{5}H, (v) domination of $\Delta L = 2$ in the reaction and, hence, the overwhelming population of the excited states, (vi) energy degeneracy of the $3/2^+$ and $5/2^+$ doublet of excited states.

The missing mass spectrum of ^{5}H obtained in this work shows a broad structure above 2.5 MeV. The observed very anisotropic correlation pattern allowed us to identify this structure as a mixture of the $3/2^+$ and $5/2^+$ states. Such a unique spin identification of the three-body system using information coming from the correlations is a novel feature

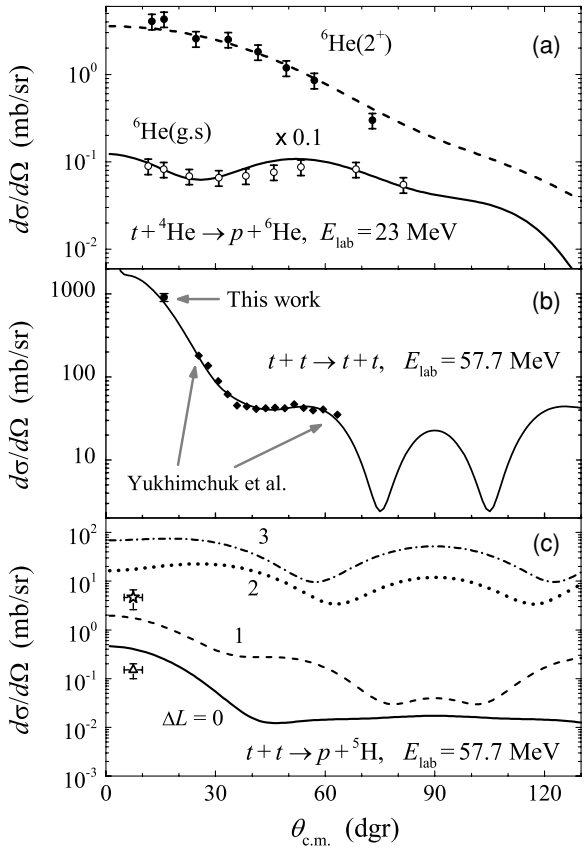

FIG. 19. (a) The DWBA calculations of the reference reaction ^{3}H(^{4}He, p)^{6}H. Data are taken from Ref. [34]. (b) The optical model fit made for the t-t elastic scattering data. Data are taken from Yukhimchuk *et al.* (Ref. [18]). (c) The DWBA calculations of the ^{3}H(t, p)^{5}H reaction for different ΔL values. The star and triangle show the experimental values of cross section for excited doublet and ground state, respectively.

of the present study. It could possibly open the way to other similar studies. The observation of sharply oscillating angular distributions is a rare phenomenon for transfer reactions involving particles with nonzero spin and is a clear evidence that the $3/2^+$ and $5/2^+$ states are almost degenerate or the

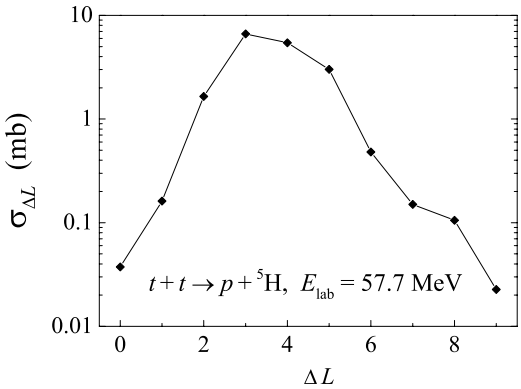

FIG. 20. DWBA calculations of the ^{3}H(t, p)^{5}H reaction: dependence of the integral cross section on the transferred angular momentum ΔL. Statistical factors are taken into account.

TABLE III. Optical-model parameters. Radial dependence of the OM potential has form $V(r) = V_0^{\rm vol} f_V(r)$, $W(r) = W_0^{\rm vol} f_W(r) + W_0^{\rm surf} g_W(r)$, where $f_i(r) = [1 + \exp(x)]^{-1}$, $x = (r - R_i)/a_i$ and $g_W(r) = 4|df_W(r)/dx|$.

Reaction	$E_{\rm c.m.}$ (MeV)	$V_0^{\rm vol}$ (MeV)	R_V (fm)	a_V (fm)	$W_0^{\rm vol}$ (MeV)	R_W (fm)	a_W (fm)	$W_0^{\rm surf}$ (MeV)	$R_W^{\rm surf}$ (fm)	$a_W^{\rm surf}$ (fm)	R_C (fm)
^{4}He + ^{3}He	13.66	−125.0	2.58	0.177	−1.6	5.40	0.800				3.29
^{4}He + ^{3}H	13.1	−100.0	2.58	0.177	−1.6	5.40	0.800				3.29
p + ^{6}He	5.6	−56.0	2.05	0.690	−1.06	1.99	0.69	−7.70	1.99	0.69	2.36
p + ^{5}H	20.1	−58.0	1.91	0.690	−2.53	1.85	0.69	−8.39	1.85	0.69	2.24
$t + t$	28.5	−57.4	2.74	0.720	−15.0	3.21	0.326				2.74

reaction mechanism causes a very specific interference of these states.

The correlation picture at $E_{^5{\rm H}} < 2.5$ MeV gives a strong indication for interference between the low-energy wing of the $3/2^+ - 5/2^+$ doublet and the $1/2^+$ ground state of ^{5}H. The ground state properties $E_{\rm g.s.} \approx 1.8$ MeV and $\Gamma_{\rm g.s.} \approx 1.3$ MeV were determined and found to be consistent with the previous studies of this reaction reported in Ref. [3]. The small observed width ($\Gamma \sim 0.5$ MeV) of the 1.8 MeV g.s. peak of ^{5}H found in Ref. [3] is the result of interference with the other states in ^{5}H in the conditions of the limited acceptance of the experimental setup employed in Ref. [3]. The present results obtained for the ^{5}H ground state are also in a good agreement with the data of Ref. [2] giving the ^{5}H g.s. at 1.7(3) MeV.

Even if the results of the present work do not solve *all* the problems of ^{5}H finally and beyond any doubt, they provide a very strong support to the location of the ^{5}H ground state at about 1.8 MeV (with a width of about 1.3 MeV) and to the presence of a doublet of practically degenerate excited states at about 5–6 MeV.

ACKNOWLEDGMENTS

We are grateful to Professor M. V. Zhukov and Professor V. Z. Goldberg for a careful reading of the manuscript and useful discussions, and to Professor V. V. Avdeichikov for assistance in the design of the detector array. This work was partly supported by the Russian Foundation for Basic Research Grant Nos. 02-02-16550, 02-02-16174, and 05-02-17535, by the INTAS Grant No. 03-51-4496, and by the Russian Ministry of Industry and Science Grant No. NS-1885.2003.2.

APPENDIX: DWBA CALCULATIONS

Code DWUCK5 [33] was used for the DWBA calculations. Adaptation of the code for our case requires (i) to consider the ^{5}H* resonant state as a slightly bound one ($E_{^5{\rm H}} = -0.1$ MeV was taken), and (ii) to assume that the two neutrons are transferred as a dineutron cluster. The dineutron wave functions for the cases of $^3{\rm H}(= p + {}^2n)$ and $^6{\rm He}(= \alpha + {}^2n)$ bound states were parametrized with the depths, radii, and diffusenesses of the binding potentials to give appropriate asymptotic behavior and realistic value for the rms matter radii of these nuclei.

To make sure that this scheme works properly we tested the model for the reactions ^{4}He(t, p)^{6}He(g.s.) and ^{4}He(t, p)^{6}He(2^+,1.8 MeV), studied in Ref. [34] at $E_{\rm lab} = 23$ MeV. The optical model (OM) potentials for the entrance and exit channels were determined in the following way. (i) Since elastic scattering data for triton on α particles at a c.m. energy around 13 MeV were not found we used, instead, data on the ^{3}He + ^{4}He elastic scattering at $E_{\rm c.m.} = 13.66$ MeV [35]. (ii) The OM parameters for the entrance channel $t + t$ at $E_{\rm c.m.} = 28.5$ MeV were extracted by a fit to the elastic scattering data obtained in the experiment [18], see Fig. 19(b). (iii) The parametrization of the global proton-nucleus optical potential CH89 [36] (neglecting its spin-orbit part) was used for the $p + {}^6$He reaction at $E_{\rm c.m.} = 5.6$ MeV to define the OM parameters for the exit channel of the ^{4}He(t, p)^{6}He* transfer reaction. (iv) The parameters of the OM potential in the exit channel and form factors of the ^{3}H and ^{5}H* bound states were chosen in the same manner as in the case of the ^{4}He(t, p)^{6}He(2^+) reaction. The parameters of the OM potentials used are given in Table III.

Numerical calculations show [see Fig. 19(a)] that the model reproduces well the data on the ^{4}He(t, p) reaction in both channels using the same OM potentials and varying only the radii of the ^{6}He(g.s.) and ^{6}He(2^+) form factors. Agreement may be obtained if the radius of the ^{6}He(2^+) form factor is taken almost two times larger than form-factor radius of ^{6}He(g.s.). The calculated cross sections for ^{3}H(t, p)^{5}H reaction at the lab energy 57.7 MeV are shown in Fig. 19(c). The dependence of these cross sections on the transferred angular momentum ΔL,

$$\sigma_{\Delta L} = 2\pi \int_{5^\circ}^{10^\circ} \frac{d\sigma_{\Delta L}(\theta)}{d\theta} \sin(\theta) d\theta,$$

is shown in Fig. 20 integrated over the angular range accessible for protons in our experiment.

[1] D. V. Aleksandrov, E. Yu. Nikol'skii, B. G. Novatskii, and D. N. Stepanov, Proceedings of the International Conference on Exotic Nuclei and Atomic Masses, Arles, France, June 19–23, 1995, p. 329.

[2] A. A. Korsheninnikov, M. S. Golovkov, I. Tanihata, A. M. Rodin, A. S. Fomichev, S. I. Sidorchuk, S. V. Stepantsov, M. L. Chelnokov, V. A. Gorshkov, D. D. Bogdanov, R. Wolski, G. M. Ter-Akopian, Yu. Ts. Oganessian, W. Mittig,

P. Roussel-Chomaz, H. Savajols, E. A. Kuzmin, E. Yu. Nikolskii, and A. A. Ogloblin, Phys. Rev. Lett. **87**, 092501 (2001).

[3] M. Golovkov, Yu. Ts. Oganessian, D. D. Bogdanov, A. S. Fomichev, A. M. Rodin, S. I. Sidorchuk, R. S. Slepnev, S. V. Stepantsov, G. M. Ter-Akopian, R. Wolski, V. A. Gorshkov, M. L. Chelnokov, M. G. Itkis, E. M. Kozulin, A. A. Bogatchev, N. A. Kondratiev, I. V. Korzyukov, A. A. Yukhimchuk, V. V. Perevozchikov, Yu. I. Vinogradov, S. K. Grishechkin, A. M. Demin, S. V. Zlatoustovsky, A. V. Kuryakin, S. V. Fil'chagin, R. I. Il'kayev, F. Hanappe, T. Materna, L. Stuttge, A. H. Ninane, A. A. Korsheninnikov, E. Yu. Nikolskii, I. Tanihata, P. Roussel-Chomaz, W. Mittig, N. Alamanos, V. Lapoux, E. C. Pollacco, and L. Nalpas, Phys. Lett. **B566**, 70 (2003).

[4] M. Meister, L. V. Chulkov, H. Simon, T. Aumann, M. J. G. Borge, Th. W. Elze, H. Emling, H. Geissel, M. Hellstrom, B. Jonson, J. V. Kratz, R. Kulessa, Y. Leifels, K. Markenroth, G. Munzenberg, F. Nickel, T. Nilsson, G. Nyman, V. Pribora, A. Richter, K. Riisager, C. Scheidenberger, G. Schrieder, O. Tengblad, and M. V. Zhukov, Nucl. Phys. **A723**, 13 (2003); Phys. Rev. Lett. **91**, 162504 (2003).

[5] M. G. Gornov, M. N. Ber, Yu. B. Gurov, S. V. Lapushkin, P. V. Morokhov, V. A. Pechkurov, N. O. Poroshin, V. G. Sandukovsky, M. V. Tel'kushev, and B. A. Chernyshev, Pis'ma Zh. Eksp. Teor. Fiz. **77**, 412 (2003) [JETP Lett. **77**, 344 (2003)].

[6] M. S. Golovkov, L. V. Grigorenko, A. S. Fomichev, S. A. Krupko, Y. T. Oganessian, A. M. Rodin, S. I. Sidorchuk, R. S. Slepnev, S. V. Stepantsov, G. M. Ter-Akopian, R. Wolski, M. G. Itkis, A. A. Bogatchev, N. A. Kondratiev, E. M. Kozulin, A. A. Korsheninnikov, E. Y. Nikolskii, P. Roussel-Chomaz, W. Mittig, R. Palit, V. Bouchat, V. Kinnard, T. Materna, F. Hanappe, O. Dorvaux, L. Stuttge, V. Lapoux, R. Raabe, L. Nalpas, A. A. Yukhimchuk, C. AnguloV. V. Perevozchikov, Y. I. Vinogradov, S. K. Grishechkin, and S. V. Zlatoustovskiy, Phys. Rev. Lett. **93**, 262501 (2004).

[7] A. A. Korsheninnikov, E. Yu. Nikolskii, E. A. Kuzmin, A. Ozawa, K. Morimoto, F. Tokanai, R. Kanungo, I. Tanihata, N. K. Timofeyuk, M. S. Golovkov, A. S. Fomichev, A. M. Rodin, M. L. Chelnokov, G. M. Ter-Akopian, W. Mittig, P. Roussel-Chomaz, H. Savajols, E. Pollacco, A. A. Ogloblin, and M. V. Zhukov, Phys. Rev. Lett. **90**, 082501 (2003).

[8] M. S. Golovkov, L. V. Grigorenko, A. S. Fomichev, Yu. Ts. Oganessian, Yu. I. Orlov, A. M. Rodin, S. I. Sidorchuk, R. S. Slepnev, S. V. Stepantsov, G. M. Ter-Akopian, and R. Wolski, Phys. Lett. **B588**, 163 (2004).

[9] N. B. Shul'gina, B. V. Danilin, L. V. Grigorenko, M. V. Zhukov, and J. M. Bang, Phys. Rev. C **62**, 014312 (2000).

[10] P. Descouvemont and A. Kharbach, Phys. Rev. C **63**, 027001 (2001).

[11] N. K. Timofeyuk, Phys. Rev. C **65**, 064306 (2002).

[12] K. Arai, Phys. Rev. C **68**, 034303 (2003).

[13] L. V. Grigorenko, N. K. Timofeyuk, and M. V. Zhukov, Eur. Phys. J. A **19**, 187 (2004).

[14] L. V. Grigorenko, Eur. Phys. J. A **20**, 419 (2004).

[15] L. K. Fifield, R. W. Zurmuhle, and D. P. Balamuth, Phys. Rev. C **8**, 2217 (1973).

[16] The idea of the method is to study the correlations of the α-particles emitted in a two-step process. The "first" emitted α particle is measured at zero degree, providing a very clear correlation picture for the "second" α particle with a distribution described by pure $|P_L(\theta)|^2$ polynomial.

[17] A. M. Rodin, S. I. Sidorchuk, S. V. Stepantsov, G. M. Ter-Akopian, A. S. Fomichev, R. Wolski, V. B. Galinskiy, G. N. Ivanov, I. B. Ivanova, V. A. Gorshkov, A. Yu. Lavrentev, andYu. Ts. Oganessian, Nucl. Instrum. Methods Phys. Res. A **391**, 228 (1997).

[18] A. A. Yukhimchuk, V. V. Perevozchikov, V. A. Apasov, V. S. Aryutkin, Yu. I. Vinogradov, M. D. Vikharev, N. S. Ganchuk, A. N. Golubkov, S. K. Grishechkin, A. M. Demin, S. V. Zlatoustovsky, G. I. Karyakin, V. A. Klisch, A. A. Kononenko, A. A. Kukolkin, A. V. Kuryakin, V. N. Lobanov, I. L. Malkov, S. S. Matveev, V. Ya. Rozhkov, V. A. Safronov, V. M. Solyankin, V. V. Travkin, D. P. Tumkin, S. V. Filchagin, Yu. Ts. Oganessian, A. M. Rodin, D. D. Bogdanov, M. S. Golovkov, A. S. Fomichev, S. I. Sidorchuk, R. S. Slepnev, S. V. Stepantsov, G. M. Ter-Akopian, and R. Wolski, Nucl. Instrum. Methods Phys. Res. A **513**, 439 (2003).

[19] I. Tilquin, Y. El Masri, M. Parlog, Ph. Collon, M. Hadri, Th. Keutgen, J. Lehmann, P. Leleux, P. Lipnik, A. Ninane, F. Hanappe, G. Bizard, D. Durand, P. Mosrin, J. Peter, R. Regimbart, and B. Tamain, Nucl. Instrum. Methods Phys. Res. A **365**, 446 (1995).

[20] K. P. Artemov, V. Z. Goldberg, I. P. Petrov, V. P. Rudakov, I. N. Serikov, V. A. Timofeev, R. Wolski, and J. Szmider, Yad. Fiz. **28**, 288 (1978) [Sov. J. Nucl. Phys. **28**, 145 (1978)].

[21] G. Cardella, A. Cunsolo, A. Foti, G. Imme, G. Pappalardo, G. Raciti, F. Rizzo, N. Alamanos, B. Berthier, and N. Saunier, Phys. Rev. C **36**, 2403 (1987).

[22] N. Glendenning, *Direct Nuclear Reactions* (Academic Press, New York, 1983).

[23] B. V. Danilin and M. V. Zhukov, Yad. Fiz. **56**, 67 (1993) [Phys. At. Nucl. **56**, 460 (1993)]; B. V. Danilin, I. J. Thompson, J. S. Vaagen, and M. V. Zhukov, Nucl. Phys. **A632**, 383 (1998).

[24] B. V. Danilin, M. V. Zhukov, A. A. Korsheninnikov, L. V. Chulkov, and V. D. Efros, Yad. Fiz. **46**, 427 (1987) [Sov. J. Nucl. Phys. **46**, 225 (1987)].

[25] O. V. Bochkarev, L. V. Chulkov, A. A. Korsheninnikov, E. A. Kuzmin, I. G. Mukha, and G. B. Yankov, Nucl. Phys. **A505**, 215 (1989).

[26] O. V. Bochkarev, A. A. Korsheninnikov, E. A. Kuzmin, I. G. Mukha, L. V. Chulkov, and G. B. Yankov, Yad. Fiz. **49**, 1521 (1989).

[27] O. V. Bochkarev, A. A. Korsheninnikov, E. A. Kuzmin, I. G. Mukha, L. V. Chulkov, and G. B. Yankov, Yad. Fiz. **55**, 1729 (1992); [Sov. J. Nucl. Phys. **55**, 955 (1992)].

[28] O. V. Bochkarev, A. A. Korsheninnikov, E. A. Kuzmin, I. G. Mukha, L. V. Chulkov, and G. B. Yankov, Bull. Rus. Acad. Sci. Phys. **57**, 183 (1993).

[29] O.V. Bochkarev, A. A. Korsheninnikov, E. A. Kuzmin, I. G. Mukha, L. V. Chulkov, and G. B. Yankov, Yad. Fiz. **57**, 1351 (1994); [Phys. At. Nucl. **57**, 1281 (1994)].

[30] L. V. Grigorenko and M. V. Zhukov, Phys. Rev. C **68**, 054005 (2003).

[31] A. A. Korsheninnikov, 41st conference on Nuclear Spectroscopy and Structure of Atomic Nuclei, Minsk, 16–19 April 1991, Book of abstracts (Leningrad, Nauka, 1991), p. 385.

[32] D. V. Aleksandrov, T. Aumann, L. Axelsson, T. Baumann, M. J. G. Borge, L. V. Chulkov, J. Cub, W. Dostal, B. Eberlein, Th. W. Elze, H. Emling, H. Geissel, V. Z. Goldberg,

A. Grunschloss, M. Hellstrom, J. Holeczek, R. Holzmann, B. Jonson, J. V. Kratz, G. Kraus, R. Kulessa, Y. Leifels, A. Leistenschneider, T. Leth, K. Markenroth, M. Meister, I. Mukha, G. Munzenberg, F. Nickel, T. Nilsson, G. Nyman, B. Petersen, M. Pfutzner, V. Pribora, A. Richter, K. Riisager, C. Scheidenberger, G. Schrieder, W. Schwab, H. Simon, M. H. Smedberg, J. Stroth, A. Surowiec, O. Tengblad, and M. V. Zhukov, Nucl. Phys. **A669**, 51 (2000).

[33] P. D. Kunz (unpublished); http://spot.colorado.edu/~kunz/DWBA.html

[34] F. Ajzenberg-Selove, E. R. Flynn, and O. Hansen, Phys. Rev. C **17**, 1283 (1978).

[35] C. G. Jacobs and R. E. Brown, Phys. Rev. C **1**, 1615 (1970).

[36] R. L. Varner, W. J. Thompson, T. L. McAbee, E. J. Ludwig, and T. B. Clegg, Phys. Rep. **201**, 57 (1991).